The Effects of Coulomb Friction on the Performance of Centrifugal Pendulum Vibration Absorbers

Brendan J. Vidmar[*], **Brian F. Feeny,**
Steven W. Shaw and Alan G. Haddow
Dynamics and Vibrations Laboratory
Department of Mechanical Engineering
Michigan State University
East Lansing, MI 48824
Email: vidmarbr@msu.edu

Bruce K. Geist
Chrysler LLC.
Auburn Hills, MI 48326
Email: bruce.geist@chysler.com

Nathan J. Verhanovitz
National Superconducting Cyclotron Laboratory
Michigan State University
East Lansing, MI 48824
Email: verhano2@msu.edu

We investigate analytically and experimentally the effects of Coulomb friction on the performance of centrifugal pendulum vibration absorbers (CPVAs), which are used to reduce torsional vibrations in rotating machinery. The analysis is based on perturbation methods applied to the non-linear equations of motion for a rotor subjected to an engine order applied torque and equipped with a circular path CPVA with viscous and Coulomb damping. The experimental work is based on quantifying parameters for the damping model using free vibration measurements with a viscous and Coulomb damping identication scheme that is enhanced to better handle measurement noise, and running tests for steady-state operation under a range of loading conditions. The level of Coulomb damping is varied by adjusting the friction of the absorber connection bearing. Good agreement is found between the analytical predictions and the experimental data. It is shown that the absorber sticks up to a level of excitation that allows it to release, after which the Coulomb damping acts in the expected manner, resulting in lowered response amplitudes. The results obtained are of general use in assessing absorber performance when dry friction is present in absorber suspensions.

1 Introduction

Centrifugal pendulum vibration absorbers (CPVAs) have been shown to significantly reduce torsional vibrations in rotating machinery that arise from engine order excitation [1–5]. Applications include internal combustion engines, helicopter rotors, turbines, and rotary aircraft engines. CPVAs have been used for several decades, having been proposed by E. S. Taylor in 1934 [6] to prevent propeller shaft failures in the Wright R-1820 engine, further developed for Curtis-Wright and Pratt & Whitney military aircraft engines [7], and since used in light aircraft engines and helicopter rotors [8]. Previous use of CPVAs in aerospace applications has been to reduce torsional vibrations of a rotor operating at a nearly constant angular velocity, denoted as Ω. Recent research has been conducted into the response and corresponding effectiveness of CPVAs for use in automotive applications, wherein Ω varies over a range of operation, and often induces transient responses [9, 10].

CPVAs are masses suspended from a rotor in such a way that they are free to move along a desired path, similar to that of a simple pendulum, for which the path is a circle. CPVAs have several inherent properties which make them ideal for use in rotating machinery. First, they have a natural frequency that scales with the rate of rotation, say $\tilde{n}\Omega$, which corresponds to a specific order of oscillation $\tilde{n}$, thereby allowing them to be tuned over a continuous range of rotor speeds. In automotive applications, the excitation order is a function of the number of cylinders being used. In a four stroke internal combustion engine, each cylinder has a cycle of two rotations, or a period of 4π radians. Thus, an N cylinder engine will have a leading order harmonic at order $\frac{N}{2}$, and the resulting rotor torque can be modeled by its dominant harmonic, $T\sin(n\theta)$, with $n = N/2$.

When tuned with $\tilde{n} \approx n$, the absorber will oscillate in a manner that passively counteracts the fluctuating applied torque acting on the rotor at the corresponding order. This

[*]Address all correspondence to this author.

works similar to the tuned translational absorber, and has the advantage that it remains tuned for all operating conditions. Lastly, these devices dissipate very little energy, and are thus very energy efficient. However, the small energy dissipated by the pendulums does have a significant effect the performance of the CPVA. In all past investigations this dissipation has been modeled as equivalent viscous damping, but in many configurations, such as the common bifilar suspension, rubbing between surfaces can occur, and thus dry friction effects may be important. In fact, sticking of absorbers has been observed in experiments, as described in this work.

Den Hartog [5] first considered non-linear effects associated with circular path CPVAs and investigated the undesired off tuning experienced by pendulum absorbers at moderate amplitudes, and the possibility of a jump instability that is disastrous for the absorber's performance. Newland [11] expanded on Hartog's idea of overtuning the pendulums in order to avoid this instability and developed a set of guidelines for choosing the tuning order. Nester [4] theoretically and experimentally investigated the steady-state circular path absorber response with an equivalent viscous damping model. Madden's patent on cycloidal paths [12] started research into alternative paths that help deal with these nonlinear effects. Denman [3] explored other paths in the context of automotive applications; he proposed a convenient two-parameter family of epicycloidal paths that includes the limiting cases of circles and Madden's cycloid, as well as a particular path, the tautochronic path, that avoids nonlinear detuning for a large, but finite, range of absorber amplitudes.

The present work extends earlier investigations by investigating the effects of dry friction. A simple Coulomb friction term is included in the equations of motion, which are treated using the method of averaging to predict the performance of the absorber in terms of the system and excitation parameters. Experiments are carried out using a rotor rig with a compound pendulum absorber, as described in [4] and below. A simultaneous viscous/Coulomb decrement method is used to accurately quantify the viscous and Coulomb damping parameters, and the method is recast to account for noise and low resolution in the experimental data. The measured system parameters are used to compare steady-state system response data with analytical predictions, and the results are found to be in good agreement.

2 Mathematical Formulations

2.1 Equations of Motion

Figure 1, depicts a schematic of a rotor/ CPVA system, where relevant parameters are defined in Table 1. The kinetic energy of this system is given by,

$$\begin{aligned} T_t = &\frac{1}{2}J_r\dot{\theta}^2 + \frac{1}{2}m\left[R^2\dot{\theta}^2 + 2RL\dot{\theta}(\dot{\theta}+\dot{\phi})\cos(\phi)\right] \\ &+ \frac{1}{2}m\left[L^2(\dot{\theta}+\dot{\phi})^2 + \rho^2(\dot{\theta}+\dot{\phi})^2\right] \end{aligned} \tag{1}$$

where J_r is the rotational inertia of the rotor, ρ is the absorber's radius of gyration about its center of mass, m is the absorber mass, and the other variables and parameters are shown in Figure 1 and listed in Table 1. Note that if the rotor lies in a horizontal plane there are no conservative forces acting on the system, and hence the potential is zero (in fact, this is a good approximation for vertical rotors as well, at least for most rotational speeds experienced in practice, for which $g << R\Omega^2$). The generalized forces associated with the damping and applied torque acting on the rotor are,

$$Q_\theta = -c_o\dot{\theta} + T_o + T\sin(n\theta)$$

where c_o is the viscous damping coefficient for the rotor bearings, T_o is the DC component of the torque, and $T\sin(n\theta)$ is the fluctuating part of the applied torque. For the absorber,

$$Q_\phi = -c_a\dot{\phi} - F_s\mathrm{sgn}(\dot{\phi})$$

where c_a is the absorber viscous damping coefficient and F_s is the magnitude of the moment acting on the absorber described by Coulomb friction. Using these results, the equations of motion are obtained using Lagrange's method. The coupled rotor and absorber equations of motion are thus given by, respectively,

$$\begin{aligned} &\left[J_r + mR^2 + m(L^2+\rho^2) + 2mRL\cos(\phi)\right]\ddot{\theta} \\ &+ m(L^2+\rho^2+RL\cos(\phi))\ddot{\phi} - mRL\dot{\phi}\sin(\phi)\left[2\dot{\theta}+\dot{\phi}\right] \\ &+ c_o\dot{\theta} = T_o + T\sin(n\theta) \end{aligned} \tag{2}$$

$$\begin{aligned} &m(L^2+\rho^2+RL\cos(\phi))\ddot{\theta} + m(L^2+\rho^2)\ddot{\phi} \\ &+ mRL\dot{\theta}^2\sin(\phi) + c_a\dot{\phi} + F_s\mathrm{sgn}(\dot{\phi}) = 0. \end{aligned} \tag{3}$$

From the vibration absorption point of view, the important quantity in Eqns.(2) and (3) is the rotor angular acceleration, $\ddot{\theta}$, which is desired to be as small as possible, implying that the rotor runs at (nearly) constant speed. This is achieved when the absorber motion imposes a torque on the rotor that (nearly) cancels the fluctuating applied torque. Due to damping, detuning, and nonlinear effects, perfect absorption is not feasible, but significant reductions in torsional vibrations can be achieved.

In order to determine the linear tuning order of the absorber, we consider the case in which the rotor is spinning at a constant speed ($\dot{\theta} = \Omega$) and absorber angles are small, in which case Eqn. (3) reduces to

$$m(L^2+\rho^2)\ddot{\phi} + mRL\Omega^2\phi + c_a\dot{\phi} + F_s\mathrm{sgn}(\dot{\phi}) = 0. \tag{4}$$

This system has an undamped natural frequency of the form $\omega_n = \tilde{n}\Omega$ where we define the linear tuning order as,

$$\tilde{n} = \sqrt{\frac{RL}{L^2+\rho^2}}.$$

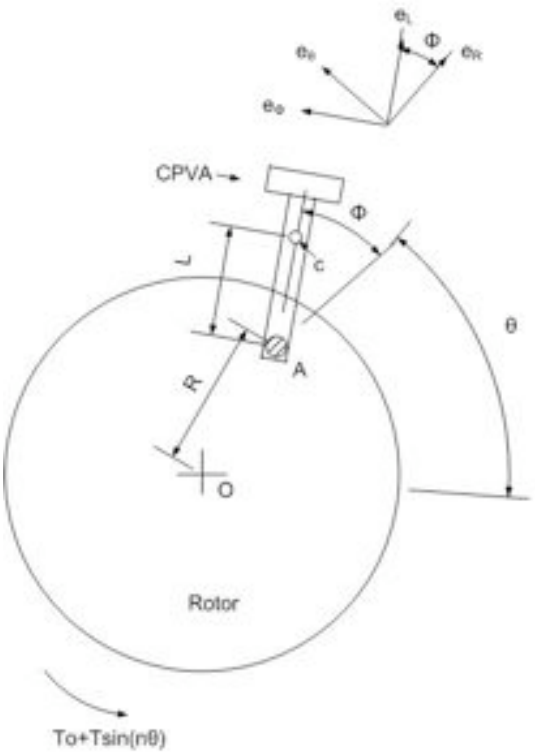

Fig. 1. Schematic of rotor and CPVA used for deriving the equations of motion.

Table 1. Definition of symbols in Fig. 1

Symbol	Physical Meaning
θ	Rotor angle
ϕ	Absorber's swing angle with respect to the rotor
R	Distance from the rotor center to the absorber's center of rotation
L	Distance from the absorber's center of rotation to its center of mass
0	Center of rotor
c	Location of the absorber's center of mass
A	Point about which the absorber swings

Note that this tuning is easily adjusted by design, but cannot be varied once realized in hardware.

2.2 Nondimensionalization and Scaling

The equations of motion (2) and (3) developed above comprise an autonomous set of differential equations due to the fact that the cyclic applied torque, $T\sin(n\theta)$, is expressed as function of the rotor angle. To perform further analysis on these equations, using the scheme described in Alsuwaiyan [1] and Nester [4], the independent variable is switched from time to θ. In order to accomplish this, a new non-dimensional variable for the rotor angular speed is defined as

$$\nu = \frac{\dot{\theta}}{\Omega} \tag{5}$$

which will be assumed to depend on θ, instead of time, as the independent variable. Note that in terms of this variable, the rotor angular acceleration is given by

$$\ddot{\theta} = \Omega^2 \nu\nu'$$

and thus $\nu\nu'$ is a nondimensional measure of the rotor torsional vibration. Similarly, the absorber angle, ϕ, is converted to a non-dimensional arc length variable

$$s = \frac{L\phi}{\beta} \tag{6}$$

that also depends on θ, where β is a length parameter which will be used to make the equations readily comparable to those derived by Alsuwaiyan [1] for general path, point mass CPVA's. Making these substitutions in Equations (2) and (3), expanding the sines and cosines to third order in s, and rearranging terms yields the non-dimensional rotor and absorber equations (Eqns. (27) and (28)), which are given in the Appendix. Derivatives are now in terms of θ, i.e., $(\,)' = d(\,)/d\theta$, and some important quantities are defined as follows, and described below:

$$\begin{aligned}
\varepsilon &= \frac{m\beta}{J_r L}(LR + L^2 + \rho^2) \\
\mu_a &= \frac{c_a}{m\Omega(L^2+\rho^2)} \\
\varphi(s') &= f_s \,\mathrm{sgn}\left(s'\right) \\
f_s &= \frac{F_s L}{m\beta\Omega^2(L^2+\rho^2)} \\
\mu_o &= \frac{c_o}{J_r\Omega} \\
\Gamma_o &= \frac{T_o}{J_r\Omega^2} \\
\Gamma(\theta) &= \frac{T}{J_r\Omega^2}\sin(n\theta).
\end{aligned} \tag{7}$$

The ε term is physically the ratio of the pendulum's inertia to that of the rotor, and will be used as the small bookkeeping parameter in the perturbation analysis. A comparison between the above equations and those in Alsuwaiyan [1] reveals that by taking $\beta = L(1+\tilde{n}^2)$, these equations are identical to those with a point mass moving along a circular path, by accounting for the moment of inertia of the absorber

pendulum about its center of mass. Parameters μ_a and f_s represent the non-dimensional viscous and Coulomb friction quantities, respectively, μ_o captures the rotor bearing viscous damping, Γ_o represents the mean applied torque, and $\Gamma(\theta)$ describes the fluctuating torque.

It has been shown by Alsuwaiyan [1] that by scaling terms in a particular way the rotor dynamics can be uncoupled, to leading order, from the absorber, allowing one to reduce the problem to essentially that of a Duffing oscillator. The required scaling is given by,

$$\begin{aligned} s &= \varepsilon^{1/2} z \\ \mu_a &= \varepsilon \tilde{\mu}_a \\ \varphi(s') &= \varepsilon^{3/2} \tilde{\varphi}(s') \\ \mu_o &= \varepsilon \tilde{\mu}_o \\ \Gamma_o &= \varepsilon \tilde{\Gamma}_o \\ \Gamma(\theta) &= \varepsilon^{3/2} \tilde{\Gamma}(\theta) \\ \nu &= 1 + \varepsilon^{3/2} w \\ \tilde{n} &= n(1 + \varepsilon\sigma) \end{aligned} \tag{8}$$

where we have taken the following terms to be small, consistent with realistic system parameters: the absorber amplitude, the absorber viscous and Coulomb dampings, the rotor damping, the mean torque, the amplitude of rotor oscillations, the applied fluctuating torque, and the detuning $\varepsilon\sigma$ between the absorber order $\tilde{n}$ and the excitation order n.

Employing these scaling assumptions in Eqn. (27), expanding, and keeping terms to order $\varepsilon^{3/2}$, yields the following equation for the non-dimensional rotor angular acceleration

$$\nu\nu' = \varepsilon^{3/2} \left(\tilde{n}^2 z + \tilde{\Gamma}(\theta) \sin(n\theta) \right) + O(\varepsilon^2), \tag{9}$$

which is desired to be made small by the absorber.

Using the above expression for the rotor acceleration, along with the scaling, allows for the rotor dynamics to be eliminated from the absorber dynamics given in Eqn. (28), resulting in the following uncoupled absorber equation of motion,

$$\begin{aligned} &z'' + n^2 z = \\ &\varepsilon(2\gamma_o z^3 - 2n^2\sigma z - f_s \operatorname{sgn}(z') - \tilde{\mu}_a z' - \tilde{\Gamma}(\theta) - n^2 z) + O(\varepsilon^{3/2}), \end{aligned} \tag{10}$$

where

$$\gamma_o = \frac{n^2}{12}(n^2+1)^2 \tag{11}$$

is the softening nonlinear stiffness coefficient associated with a circular path absorber. By varying γ_o one can study a parameterized family of paths [1].

2.3 Perturbation Analysis

To obtain approximate solutions to the absorber equations of motion (10), the method of averaging is applied. To begin, we express the absorber motion in polar coordinates of the form

$$z(\theta) = a(\theta)\sin(n\theta + \alpha(\theta)) \tag{12}$$

$$z'(\theta) = na(\theta)\cos(n\theta + \alpha(\theta)) \tag{13}$$

where a and α are the amplitude and phase of the absorber response which, under our assumptions, will be slowly varying functions of θ. Applying the method of averaging yields the following equations that govern the averaged values of (a, ϕ) to leading order in ε,

$$\bar{a}' = \varepsilon \left(-\frac{\tilde{\mu}_a}{2}\bar{a} - \frac{2f_s}{\pi} + \frac{\tilde{\Gamma}(\theta)}{2n}\sin\bar{\alpha} \right) \tag{14}$$

$$\bar{a}\bar{\alpha}' = \varepsilon \left(-\frac{3\gamma_o}{4n}\bar{a}^3 + n\bar{a}(\sigma + \frac{1}{2}) + \frac{\tilde{\Gamma}(\theta)}{2n}\cos\bar{\alpha} \right). \tag{15}$$

The constant steady state amplitude and phase, $\bar{a} = a_{ss}$ and $\bar{\alpha} = \alpha_{ss}$, are determined by solving for the zeros of these equations, which satisfy,

$$\frac{\tilde{\Gamma}}{2n}\sin\alpha_{ss} = \frac{\tilde{\mu}_a}{2}a_{ss} + \frac{2f_s}{\pi} \tag{16}$$

$$\frac{\tilde{\Gamma}}{2n}\cos\alpha_{ss} = \frac{3\gamma_o}{4n}a_{ss}^3 - na_{ss}(\sigma + \frac{1}{2}). \tag{17}$$

Using $(\tilde{\Gamma}\cos\alpha_{ss})^2 + (\tilde{\Gamma}\sin\alpha_{ss})^2 = \tilde{\Gamma}^2$ the steady state phase can be eliminated from Eqns. (16) and (17), resulting in the following relationship between the amplitude of the fluctuating torque $\tilde{\Gamma}$ and the steady-state absorber amplitude,

$$\tilde{\Gamma}^2 = \left(\frac{\tilde{\mu}_a}{2}a_{ss} + \frac{2f_s}{\pi} \right)^2 + \left(\frac{3\gamma_o}{4n}a_{ss}^3 - na_{ss}(\sigma + \frac{1}{2}) \right)^2. \tag{18}$$

Once a_{ss} is obtained from this expresssion, Eqns. (16) and (17) can be used to recover the corresponding phase α_{ss}.

A useful result immediately available from Eqn.(18) is the torque level needed for the absorbers to overcome the dry friction and begin to move. This is obtained by letting $a_{ss} = 0$, from which we find the following torque amplitudes, expressed in terms of non-dimensional and physical parameters, respectively, that are required for the absorbers to begin to oscillate:

$$\tilde{\Gamma} > \tilde{\Gamma}^* = \frac{2f_s}{\pi} \quad T > T^* = \frac{F_s J_r}{m(L^2 + R^2 + RL)}. \tag{19}$$

2.4 Analytical Steady-State Results

Equations (9) and (18) allow for investigations of the effects of Coulomb friction on the steady-state system response. In order to demonstrate the general effects of Coulomb friction, we first show sample response plots for a system with and without Coulomb friction. Figure 2 displays the non-dimensional absorber amplitude $|s|$ and non-dimensional rotor angular acceleration $|\nu\nu'|$ as functions of the non-dimensional fluctuating torque amplitude $\tilde{\Gamma}$ for models with and without Coulomb damping, with parameter values taken from the experimental study described subsequently. It should be noted that in all of the subsequent plots exhibiting the rotor angular acceleration, the active absorber does not achieve the level of vibration reduction which is commonly required in applications. This is due to a very small ratio of absorber inertia to that of the rotor ($\approx 1.5\%$) in the experimental rig, which could easily be increased through the use of additional absorbers. As the intention of this paper is to analyze the effects of Coulomb friction on the absorber this practicality will be of minor importance here.

Referring back to Figure 2, it is seen that with Coulomb friction present, the absorber sticks up to the threshold $\tilde{\Gamma}^* \approx 0.002$, after which point the absorber is released. During the sticking phase the rotor angular acceleration follows the reference line that corresponds to the case with the absorber locked at its zero position. Once the absorber is released, its motion initially causes the torsional vibrations to flatten out as $\tilde{\Gamma}$ is increased, until nonlinear effects take over and the vibration levels begin to increase slightly, after which an instability occurs, as described next. From Figure 2 (a) it is evident that as $\tilde{\Gamma}$ increases, the absorbers go unstable (indicated by the dotted lines) and a jump occurs. This jump is accompanied by a π radian shift in the phase between the absorber and the rotor. This phase shift of the absorber results in an increase in the torsional vibrations on the rotor. This is the undesired instability first investigated by Newland [11], and its effects on torsional vibrations can be observed by plotting the rotor angular acceleration amplitude against $\tilde{\Gamma}$, as shown in Figure 2 (b). For reference, the linear viscously damped as well as the linear undamped rotor angular acceleration response are shown. As evident, the rotor acceleration is exactly zero for the linear, conservative, perfectly tuned absorber. The linear rotor response with absorber damping is a straight line tangent to the non-linear, viscously damped response at the origin. In fact, in the linear case, only damping and detuning cause the rotor response to be nonzero. The non-linear conservative rotor response is tangent to the zero rotor angular acceleration axis, until the nonlinearities are prominent, and the absorber begins to amplify at a critical torque level which is less than the damped version. One can identify the damping effects on the absorber by looking at Eqn. (19). In summary, Figure 2 (b) shows that the linear rotor response is zero for the undamped case, and increases with the addition of viscous damping. The pendulum nonlinearity causes an onset of instability when the amplitude of fluctuating torque exceeds a critical level. Coulomb damping in the nonlinear system degrades the absorber performance relative to the viscously damped system, but increases the torque range below the amplifying instability. These trends carry over for small amounts of detuning. The linear equations of motion are presented for reference in Appendix B.

In practice, the absorbers are commonly overtuned ($\tilde{n} > n$) in order to allow for a wider range of torques. Shown in Figure 3 are the absorber amplitude and rotor angular acceleration, in terms of analytical predictions and simulations of the nonlinear equations of motion, plotted against $\tilde{\Gamma}$ for different values of σ, the absorber detuning. One can see that choosing the level of detuning is a design problem, since larger levels of detuning allow for the absorber to operate in the stable region for a wider range of torque, but they also slightly reduce the effectiveness of the absorbers, in terms of reducing torsional vibrations.

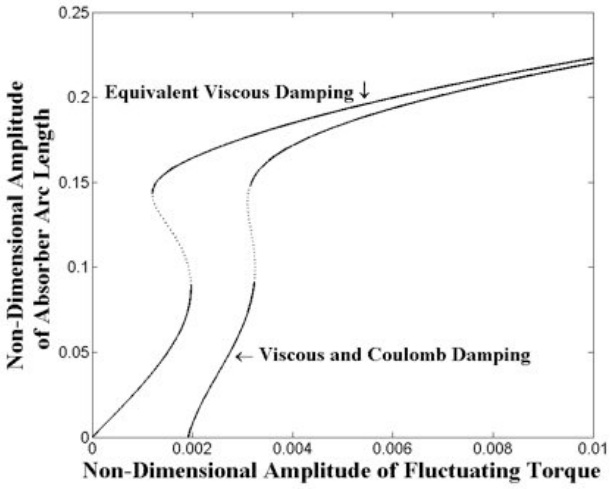

(a)

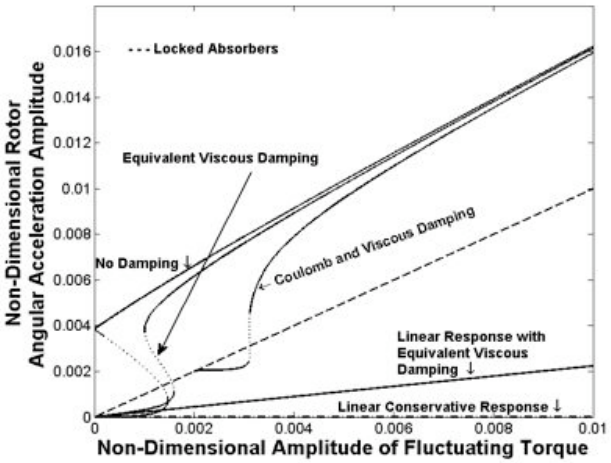

(b)

Fig. 2. (a) Non-dimensional absorber amplitude vs. non-dimensional fluctuating torque amplitude for the different damping models and $\sigma = 0$. (a_{ss} vs. Γ), (b) Non-dimensional rotor acceleration amplitude vs. non-dimensional fluctuating torque amplitude for the different damping models and $\sigma = 0$. ($\nu\nu'$ vs. Γ).

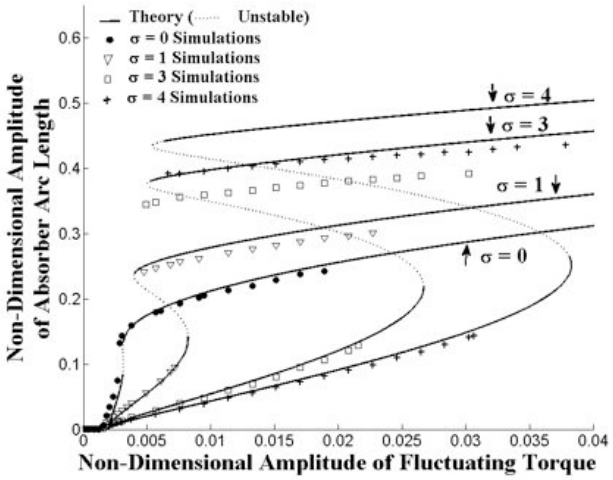

(a)

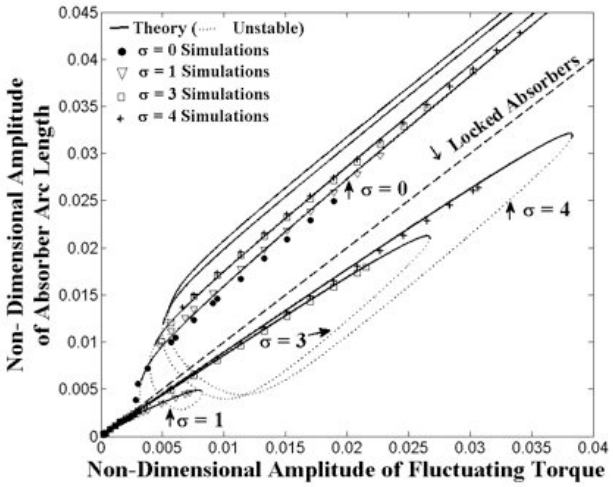

(b)

Fig. 3. (a) Non-dimensional absorber amplitude vs. non-dimensional fluctuating torque amplitude for different levels of detuning. (a_{ss} vs. Γ), (b) Non-dimensional rotor acceleration amplitude vs. non-dimensional fluctuating torque amplitude for different levels of detuning. ($\nu\nu'$ vs. Γ)

Figure 4 depicts the effects of varying Coulomb friction on the system response in terms of analytical predictions and simulations. Figures 4 (a,b) display the steady-state amplitudes of the absorber and the rotor angular acceleration versus $\tilde{\Gamma}$ for three different damping conditions, with 4% ($\sigma = 3$) absorber overtuning. Here cases A, B, and C represent different levels of viscous and Coulomb damping, given in Table 2, which are selected to match experimental results. It is seen that increased levels of Coulomb friction allows for a larger torque to be applied to the rotor before the absorber goes unstable. As noted above, the absorber "sticks" for a range of torques and the rotor angular acceleration is that of the system with the absorber locked at zero. As the level of Coulomb friction is increased, it takes a greater level of fluctuating torque to achieve absorber oscillation. This is confirmed in Figure 4(a), which shows that as the level of Coulomb friction is increased, the absorber sticks for a larger level of fluctuating torque, and the response becomes unstable at a larger torque levels. However, from Figure 4 (b) it is also seen that as the absorber sticks for larger values of torque, it is not effective as an absorber in terms of reducing rotor torsional vibrations.

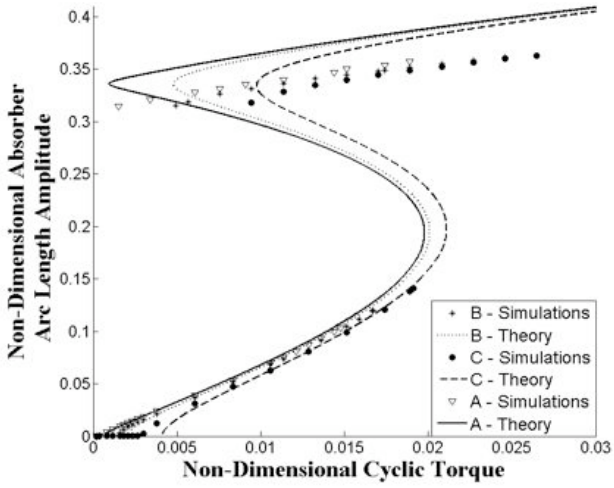

(a)

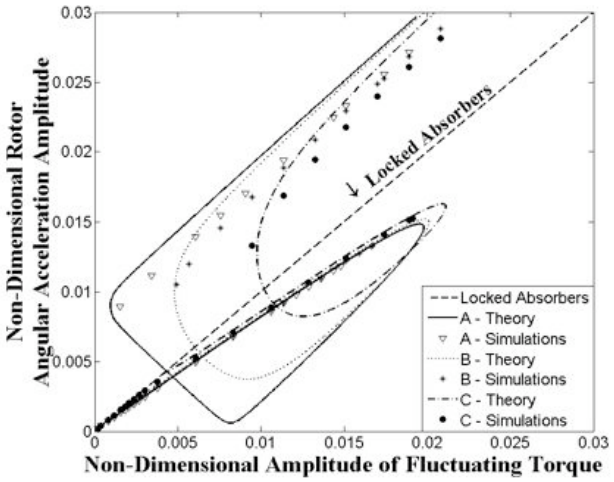

(b)

Fig. 4. (a) Non-dimensional absorber amplitude vs. fluctuating torque amplitude for different levels of Coulomb friction and 4% detuning. (a_{ss} vs. Γ), (b) Non-dimensional rotor acceleration amplitude vs. non-dimensional fluctuating torque amplitude for different levels of Coulomb friction and 4% detuning. ($\nu\nu'$ vs. Γ)

2.5 Experimental Investigation

The experimental rig consists of a shaft (the rotor) with a mounting section for up to four absorbers, driven by a controlled electric motor. For the present study the setup is equipped with one free absorber, as well as balance masses

Table 2. Damping Values Associated with Letters A, B, and C in Figures 4, 7 and 8.

Letter	β	x_k
A	0.000268	0.0354
B	0.0025	0.1077
C	0.0051	0.218

that can be used to vary the inertia of the rotor (and hence ε). A photo of the experimental rig, a schematic diagram of the experimental setup, and photo of the experimental circular path CPVA, consisting of a "T"-shaped compound pendulum, are shown in Figure 5. The instantaneous angle of the absorber ϕ is measured via an optical encoder. The instantaneous rotor speed $\dot{\theta}$ is also measured by an optical encoder, from which the mean and harmonic components, as well as the angular acceleration, can be distilled. The torque $T(\theta)$ applied to the rotor is supplied by an input voltage to the armature, and is quantified by measuring the current produced by the spinning of the rotor; a current to voltage conversion is set in the control box which allows the corresponding torque voltage to be displayed in Labview. Using the inertial properties of the motor given by the manufacturer, the torque (in Newton-meters) can then be obtained from the voltage measurement. All three of these signals (absorber angle, rotor speed, and torque) are fed into a PC running data acquisition and control software (coded in LabVIEW), which allows for real-time viewing and post-processing of data in the time or order (frequency divided by the mean speed) domains. The custom written LabVIEW code also allows for PID feedback control of the mean rotor speed to maintain a nearly constant mean speed, upon which the fluctuating torque is applied. Further details of this rig are described in [13].

The first set of experiments described are from free vibrations of the absorber, which are initiated by shutting off a resonant fluctuating torque and letting the absorbers ring down, while maintaining nearly constant rotor speed. These results are used to measure the absorber damping parameters. A set of steady-state runs are then carried out under different loading and tuning conditions, for different levels of absorber bearing friction, and the measured response results are compared with the predictions obtained from the perturbation analysis.

(a)

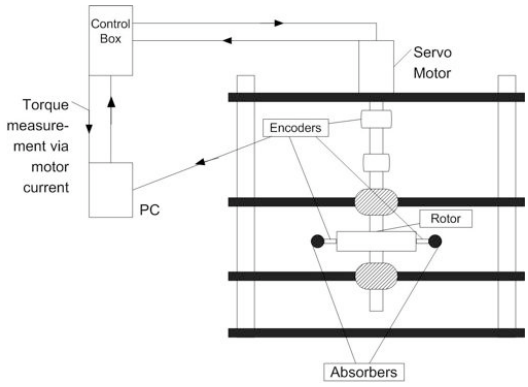

(b)

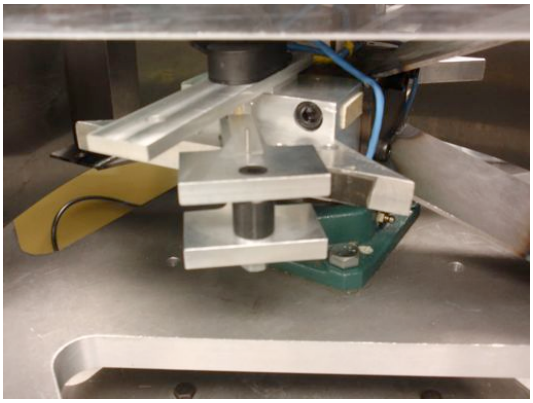

(c)

Fig. 5. (a) Photo of experimental rig (b) Schematic of experimental rig (c) Photo of experimental circular path absorber

2.6 Experimental Identification of Damping Parameters

In order to compare theoretical and experimental results, the effective viscous and Coulomb friction damping values associated with the experimental absorber must be determined. The primary source of this damping is resistance in a roller bearing that supports the pivot of the absorber pendulum. To estimate these parameters, a scheme by Liang and Feeny [14] is adopted, in which the parameters are determined from free vibration information. This is accomplished by solving the piecewise linear, single degree of freedom oscillator equation, Eqn. (4), in a piecewise manner with viscous and Coulomb damping, for consecutive extrema of the free vibration response, denoted here as X_i. From this solution one can derive the following recursive relationship:

$$X_i = -e^{-\beta\pi}X_{i-1} + (-1)^{i-1}(e^{-\beta\pi}+1)x_k, \qquad i = 1,2,.....,n \tag{20}$$

where β contains the viscous component ($\beta = \zeta/\sqrt{1-\zeta^2}$) where $\zeta = c_a/2m_{eff}\omega_n$, with $m_{eff} = m(L^2+\rho^2)$ and $\omega_n =$

$\tilde{n}\Omega$, and the Coulomb friction is contained in $x_k = F_s/k_{eff}$, where $k_{eff} = mRL\Omega^2$ is the effective stiffness due to centrifugal effects. To isolate the viscous damping coefficient, we sum successive expressions for X_i's; computing $X_i + X_{i+1}$ and canceling and rearranging terms yields,

$$\frac{X_i + X_{i+1}}{X_{i-1} + X_i} = -e^{-\beta\pi} \tag{21}$$

from which one can determine β. Once β is found, x_k can be obtained using Eqn. (20), from which one determines the magnitude of the dry friction torque acting on the absorber, $F_s = mRL\Omega^2 x_k$.

The expressions for computing β (Eqn. (21)) and x_k (Eqn. (20)) make use of 3 consecutive measurements of local peaks in the free vibration response. If there is noise in the system and/or uncertainty in the measurements, the precision degrades. To deal with this, we can generalize Eqn. (20) to allow a range of $i+m$ half cycles to i half cycles (achieved by expanding Eqn. (20) and substituting in the expression for X_{i-1}), such that

$$X_{i+m} = (-1)^m e^{-m\beta\pi} X_i + (-1)^{i+m-1}(e^{-\beta\pi}+1)x_k \sum_{j=1}^{m} e^{-(m-j)\beta\pi}. \tag{22}$$

This allows for a measurement over a range of m half cycles, resulting in,

$$\frac{X_m + X_{i+m}}{X_{i-1} + X_i} = -e^{-m\beta\pi}. \tag{23}$$

Which allows for the full range of decay to be used. This can be further improved if we let $i \rightarrow i+n$, in which case the measurement of consecutive half-cycles can be avoided all together. Doing this we obtain the cases,

$$\frac{X_{i+m} - X_{m+n+i}}{X_i - X_{i+n}} = (-1)^m e^{-m\beta\pi} \qquad n \text{ even} \tag{24}$$

for the case when both measurements are maxima (or both minima), and

$$\frac{X_{i+m} + X_{m+n+i}}{X_i + X_{i+n}} = (-1)^m e^{-m\beta\pi} \qquad n \text{ odd} \tag{25}$$

when the measurements are one each of maxima and minima. In these expressions the numerators and denominators mark the differences in extrema over n half cycles, and the ratios express how these differences are changing over a decay of m half cycles. Similarly to the single cycle case, β can be estimated from either Eqn. (24) or (25), and then then x_k (F_s) can be found from Eqn. (22). If $m = n$ then we need only 3 measurements, which can be taken to cover a wide span of decaying oscillations. These generalizations help improve the accuracy of the decrement scheme by allowing one to capture data from the entire range of free vibration (m), as well as by spreading consecutive measurements to a wider range (n), which helps deal with low resolution in the measurements.

To perform the free vibration analysis on the test rig, the rotor was spun up to a speed of 350 RPM, and an oscillating torque was applied on top of the mean torque to initiate an absorber response. Once the absorber was oscillating at a desired amplitude, the oscillating torque was immediately turned off, leaving only the mean torque on the rotor. The absorber was then in a free vibration mode, decaying in amplitude due only to the damping components. In order to determine β and x_k values from the data, an $m+n$ was chosen that covered the entire range of the response with m and n values directly in the middle of the response ($m, n = 25$ half cycles). This yielded $\beta = 0.0025$ and $x_k = 0.1077$, which were then used in the simulated free vibration response for comparison with the experimental data, as shown in Fig. 6. It should be noted that the viscous and Coulomb parameters are estimated assuming a linear stiffness, which is true of the absorber for small angles, and assuming single degree of freedom dynamics. The experimental free vibration was conducted from a maximum absorber swing angle of $\pm 16^\circ$, and the rotor-speed controller is assumed to isolate the rotor from the absorber, thereby letting it behave as essentially a single degree of freedom system. The simulations used to compare the identified damping parameters against the experimental results are from the fully non-linear, coupled equations, Eqns. (2) and (3), which confirms the validity of the assumptions.

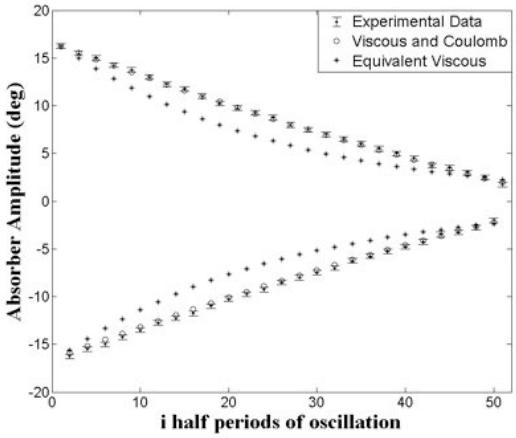

Fig. 6. Theoretical vs. experimental free vibration peak values for small amplitudes

It is evident from Figure 6 that the parameters extracted from the simultaneous viscous/Coulomb method track the experimental transient decay data very closely, verifying that the absorber damping is accurately described by the proposed model. The relatively small value of the equivalent viscous damping model predicts much more damping than

seems to be present. To quantify how well this data fits the model we consider residuals. To define the residual for this case, we denote $\tilde{X}_i$ as the amplitude of the response predicted by the estimated damping coefficients to be, and X_i as the measured amplidute. The residual is then defined by the normalized quantity,

$$r = \frac{\tilde{X}_i - X_i}{|X_i|}. \tag{26}$$

To minimize resolution effects, we computed this residual for every 4 half periods. For the identified Coulomb plus viscous model, it was found that r was randomly scattered and bounded in the range $-0.01 < r < 0.03$ over 14 response half-cycles, indicating the validity of the model [15].

3 Experimental Steady-State Results

Steady-state absorber tests were conducted to assess the predictive capabilities of the perturbation results. The levels of friction acting on the absorber were changed via tightening and loosening the support bolt at the pivot about which the absorber rotates, resulting in changes in both the Coulomb and viscous friction coefficients. For each level of friction, the previously explained damping estimation method was utilized to quantify the amounts of Coulomb friction and viscous damping.

Figures 7 and 8 summarize the results for the steady state absorber and rotor responses, respectively, both plotted versus the torque amplitude Γ for 4% detuning ($\sigma = 3$). Response curves are provided for three different levels of Coulomb damping, indicated on the graphs by letters A, B, and C, where the respective damping values are given in Table 2. Figure 7 compares experimental data versus the averaged equation solution. The hysteresis/jump phenomenon is clearly exhibited in the experimental data: sweeping up the torque causes the absorber amplitude to jump to the upper solution branch; similarly, while sweeping back down, the absorber amplitude stays on the upper branch until jumping to the lower branch, with a range of bistability between the jump conditions. Examination of Figure 7 reveals that the experimental data follows the theoretical curves in a qualitative sense, and offer reasonable quantitative agreement. The absorber is observed to stick for different ranges of the applied torque, corresponding to the different friction levels, as predicted. Some error between the data and the theory is observed, especially on the upper solution branch, but this can be attributed to the perturbation theory, which assumes small pendulum angles.

Figure 8 displays the angular acceleration of the rotor versus the applied fluctuating torque, comparing experimental measurements with theoretical predictions. A reference line is also plotted which conveys the predicted rotor angular acceleration if the absorbers are locked. It is obvious that increasing the friction causes the absorber to oscillate less, thus decreasing its performance in the stable regime. The increase in friction does, however, enable the absorber to remain stable over a larger range of fluctuating torque. It is seen in Figure 8 that as the absorber becomes unstable and jumps to the upper solution branch, it begins to increase the torsional vibrations of the rotor, as predicted.

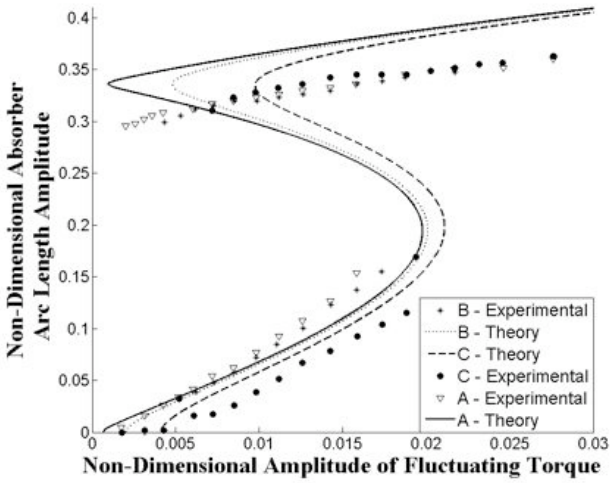

Fig. 7. Experimental and theoretical non-dimensional absorber arc length vs. non-dimensional amplitude of fluctuating torque for 4% detuning and different levels of Coulomb friction. (a_{ss} vs. Γ)

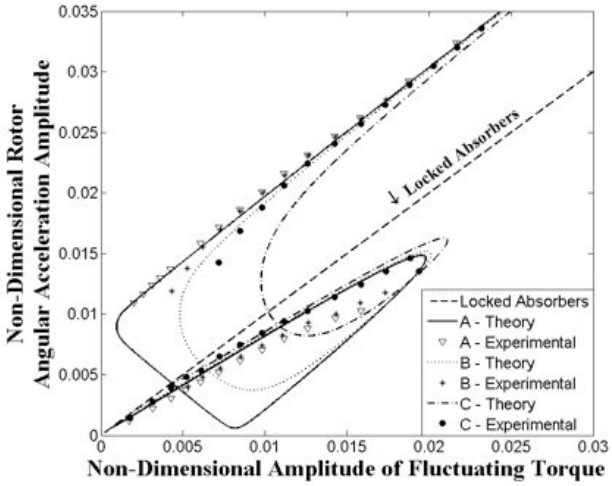

Fig. 8. Experimental and theoretical non-dimensional amplitude of rotor angular acceleration vs. non-dimensional amplitude of fluctuating torque for 4% detuning and different levels of Coulomb friction. ($\nu\nu'$ vs. Γ)

4 Conclusions

In this work, we examined the effects of Coulomb (dry) friction on the response of a rotor/absorber system. The investigation considered and compared results from the full

equations of motion, a perturbation analysis, and experimental measurements. The validity of the perturbation results was confirmed via simulations of the fully non-linear equations of motion, and they were also shown to be an adequate predictor for experimental results. The amount of Coulomb friction was varied in the experimental study and quantified through a modified simultaneous viscous/Coulomb decrement scheme; this method was found to accurately identify the viscous and Coulomb damping parameters, and it verified that the viscous/Coulomb model correctly describes the damping mechanisms of the absorber. Steady-state tests were conducted at the different friction levels, and it was confirmed that the mathematical model accurately describes the effects of friction. Specifically, the Coulomb friction was shown to cause the absorbers to stick for a range of applied torque, as well as to increase the level of fluctuating torque at which jumps in the response occurred (as expected, due to the increased dissipation). The sudden jump in absorber amplitude was captured experimentally and the detrimental effect that this has on the absorber's performance was also observed. It was predicted and observed that Coulomb friction has a greater effect at small absorber amplitudes, and at smaller detuning levels, as expected, since Coulomb friction dominates over viscous damping at small amplitudes of oscillation. The present study provides a quantitative model for predicting such results, which are of use when considering absorber systems with suspensions that involve dry friction.

5 Acknowledgement

This material is based on work supported by the National Science Foundation under Grant No. CMS-0700307. Any findings, opinions, conclusions or recommendations are those of the authors and do not necessarily reflect the views of the NSF. The authors are grateful to Ryan Monroe for useful discussions related to this work.

6 Appendix A

The non-dimensional rotor and absorber equations of motion, as developed in Section 2.2, are given by the following, in which the independent variable is θ:

$$\left[1+\frac{m}{J}(L^2+R^2+\rho^2)+\frac{2mLR}{J}-\frac{mR\beta}{JL}s^2\right]\nu\nu' + \left[\varepsilon-\frac{mR\beta^3}{2JL^2}s^2\right]\left[\nu\nu's'+\nu^2s''\right]-\frac{mR\beta^3}{JL^2}(\nu s')^2\left[s-\frac{\beta^2}{6L^2}s^3\right] - \frac{mR\beta^2}{JL}\nu^2s'\left[2s-\frac{\beta^2}{3L^2}s^3\right]+\mu_o\nu=\Gamma_o+\Gamma(\theta)+HOT \tag{27}$$

$$s'\nu'\nu+\nu^2s''+\frac{LR}{L^2+\rho^2}\left[s-\frac{\beta^2}{6L^2}s^3\right]\nu^2 \frac{L^2R}{\beta(L^2+\rho^2)}\left[-\frac{1}{2}\left(\frac{\beta s}{L}\right)^2+\frac{L^2+LR+\rho^2}{L}\right]\nu\nu' + \mu_a s'\nu+\varphi(s')+HOT=0 \tag{28}$$

where HOT refer to higher order terms in s.

7 Appendix B

For small absorber amplitudes, $\|\phi\| \ll 1$, and small fluctuations of the rotor about a constant speed,

$$\theta=\Omega t+\vartheta$$

and retaining linear terms, Eqns.2 and 3 reduce to:

$$\left[J+m((R+L)^2+\rho^2)\right]\ddot{\vartheta}+m(RL+L^2+\rho^2)\ddot{\phi}=T\sin(n\Omega t) \tag{29}$$

$$m(LR+r^2+\rho^2)\ddot{\vartheta}+m(L^2+\rho^2)\ddot{\phi}+mLR\Omega^2\phi+c_a\dot{\phi}=0 \tag{30}$$

References

[1] Alsuwaiyan, A. S., 1999. "Performance, stability, and localization of systems of vibration absorbers". PhD thesis, Michigan State University.

[2] Chao, C. P., and Shaw, S. W., 2000. "The dynamic response of multiple pairs of subharmonic torsional vibration absorbers". *Journal of Sound and Vibration,* **231**, pp. 411–431.

[3] Denman, H. H., 1992. "Tautochronic bifilar pendulum torsion absorbers for reciprocating engines". *Journal of Sound and Vibration,* **159**, pp. 251–277.

[4] Nester, T. M., 2002. "Experimental investigation of circular path centrifugal pendulum vibration absorbers". Master's thesis, Michigan State University.

[5] Den Hartog, J. P., 1985. *Mechanical Vibrations*. Dover Publications, Inc. New York.

[6] Den Hartog, J. P., 1937. "Vibration in industry". *Journal of Applied Physics,* **8**, pp. 76–83.

[7] McCutchen, K. D., 2001. "No short days. the struggle to develop the r-2800 "double wasp" crankshaft". *Journal of the American Aviation Historical Society,* **Summer**, pp. 124–146.

[8] KerWilson, 1968. *Practical Solutions of Torsional Vibration Problems*. Chapman and Hall, Ltd., London.

[9] S.W. Shaw, M.B. Orlowski, A. H., and Geist, B., 2008. "Transient dynamics of centrifugal pendulum vibration absorbers". In Proceedings of the 12th International Symposium on Transport Phenomena and Dynamics of Rotating Machinery, no. 2008-20119.

[10] Nester, T., Haddow, A., Shaw, S., Brevick, J., and Borowski, V., 2003. "Vibration reduction in variable displacement engines using pendulum absorbers". In Proceedings of the SAE Noise and Vibration Conference and Exhibition.

[11] Newland, D. E., 1964. "Nonlinear aspects of the performance of centrifugal pendulum vibration absorbers". *ASME Journal of Engineering for Industry,* **86**, pp. 257–263.

[12] Madden, J., 1980. Constant frequency bifilar vibration absorber. Tech. rep., United States Patent No. 4218187.

[13] Shaw, S. W., Schmitz, P. M., and Haddow, A. G., 2006. "Dynamics of tautochronic pendulum vibration absorbers: Theory and experiment.". *Journal of Computational and Nonlinear Dynamics,* **1**, pp. 283–293.

[14] Liang, J. W., and Feeny, B. F., 1998. "Identifying Coulomb and viscous friction from free-vibration decrements". *Nonlinear Dynamics,* **16**, pp. 337–347.

[15] Beck, J., and Arnold, K., 1977. *Parameter Estimation*. Wiley.